Dynamics of an Axially Moving Bernoulli-Euler Beam : Spectral Element Modeling and Analysis

Hyungmi Oh
Graduate School, Department of Mechanical Engineering, Inha University, Incheon 402-751, Korea
Usik Lee*
Professor, Department of Mechanical Engineering, Inha University, 253 Yonghyun-Dong, Nam-Ku, Incheon 402-751, Korea
Dong-Hyun Park
Associate Professor, Department of Industrial Engineering, Inha University, Incheon 402-751, Korea

The spectral element model is known to provide very accurate structural dynamic characteristics, while reducing the number of degree-of-freedom to resolve the computational and cost problems. Thus, the spectral element model for an axially moving Bernoulli-Euler beam subjected to axial tension is developed in the present paper. The high accuracy of the spectral element model is then verified by comparing its solutions with the conventional finite element solutions and exact analytical solutions. The effects of the moving speed and axial tension on the vibration characteristics, wave characteristics, and the static and dynamic stabilities of a moving beam are investigated.

Key Words : Moving Beam, Vibration, Spectral Element Model, Natural Frequency, Critical Moving Speed, Divergence, Flutter

1. Introduction

The moving belts used in power transmission are an example of a class of axially moving structures. Axially moving speed may significantly affects the dynamic characteristics of moving structures even at low speed, giving rise to the variation of natural frequencies and complex modes. Above a certain critical moving speed, axially moving structures may experience severe vibrations, static instability, or dynamic instability to result in structural failures. Thus, it is important to accurately predict the dynamic characteristics and instability of such structures in advance for the successful analysis and design of a broad class of technological devices. The literature regarding axially moving structures is quite wide, and an extensive literature overview can be found in Wickert and Mote (1988).

The axially moving beam-like one-dimensional structure with flexural rigidity has been traditionally represented by the Euler-Bernoulli beam (BE-beam) model or Timoshenko beam model. The solutions of the equations of motion for the moving beam models have been obtained by various solution techniques including the Galerkin's method (Hwang and Perkins, 1992 ; Al-Jawi et al., 1995 ; Pellicano and Vestroni, 2001), assumed mode method (Lee, 1993), finite element method (FEM) (Stylianou and Tabarrok, 1994), Green's function method (Wickert and Mote, 1990), transfer function method (Riedel and Tan, 1998), perturbation method (Öz, 2001), and the Laplace

* Corresponding Author,
E-mail : ulee@inha.ac.kr
TEL : +82-32-860-7318; **FAX** : +82-32-866-1434
Department of Mechanical Engineering, Inha University, 253 Yonghyun-Dong, Nam-Ku, Incheon 402-751, Korea. (Manuscript **Received** June 3, 2003; **Revised** December 16, 2003)

Copyright (C) 2003 NuriMedia Co., Ltd.

transform method (Chonan, 1986).

In the literature (Doyle, 1997; Lee and Lee, 1998; Lee et al., 2000, 2001), it has been well recognized that the spectral element method (SEM) is an exact solution method for the dynamic analysis of structures. In SEM, the spectral element matrix (or exact dynamic stiffness matrix) is formulated in frequency-domain by using exact dynamic shape functions. Therefore it does not require any structural discretization to improve the solution accuracy for a uniform beam, regardless of its length. As it is one of element methods, the conventional finite element assembly procedure can be equally applied to formulate the global system dynamic equation of a structure. In SEM, the dynamic responses in frequency- and time-domains are computed very efficiently by using the forward-FFT (simply, FFT) and inverse-FFT (simply, IFFT) algorithms. Recently, Le-Ngoc and McCallion (1999) derived the dynamic stiffness matrix for the axially moving string to obtain exact eigenvalues. However, the spectral element model in terms of exact dynamic stiffness matrix has not been introduced in the literature for axially moving beam structures.

The purposes of the present paper are first to formulate the spectral element model for the transverse vibration of an axially moving BE-beam model subjected to an axial tension, and then to verify its high accuracy by comparing with the solutions by the other solutions methods, and finally to investigate the effects of the moving speed and axial tension on the vibration and stability of the moving beam.

2. Equation of Motion

Consider a BE-beam model of flexural rigidity EI, which travels under an applied axial tension P with constant transport speed c. The equation of motion and relevant boundary conditions can be derived form the extended Hamilton's principle

$$\int_{t_1}^{t_2}(\delta K-\delta V+\delta W)\,dt=0 \tag{1}$$

where K and V are the kinetic energy and the potential energies, respectively, and δW is the virtual work. The kinetic and potential energies are given by

$$\begin{aligned} K&=\frac{1}{2}\int_0^L \rho A\{c^2+(\dot{w}+cw')^2\}dx \\ V&=\frac{1}{2}\int_0^L (EIw''^2+Pw'^2)\,dx \end{aligned} \tag{2}$$

where $w(x, t)$ is the transverse deflection, L is the length of beam and ρA is the mass per length of beam. In Eq. (2), the dot $(\cdot)$ and prime $(')$ denote the derivatives with respective to time and spatial coordinate x, respectively. The virtual work δW is given by

$$\begin{aligned} \delta W=&\int_0^L f(x, t)\,\delta x+M_1\delta\theta_1+M_2\delta\theta_2 \\ &+Q_1\delta w_1+Q_2\delta w_2 \end{aligned} \tag{3}$$

where $f(x, t)$ is the external force and (M_1, M_2), (Q_1, Q_2) and (θ_1, θ_2) are the bending moments, shear forces, and slopes specified at two boundaries of $x=0$ and $x=L$, respectively. The slopes θ_1 and θ_2 are related to the transverse deflection as

$$\theta_1(t)=w'(0, t),\ \theta_2(t)=w'(L, t) \tag{4}$$

Introducing Eqs. (2) and (3) into the extended Hamilton's principle, Eq. (1), and applying the integral by parts yields

$$\begin{aligned} &\int_{t_1}^{t_2}\int_0^L\{-EIw''''-\rho A(c^2w''+2c\dot{w}'+\ddot{w}) \\ &\qquad+Pw''+f(x, t)\}\delta w\,dx\,dt \\ &+\int_{t_1}^{t_2}\{-Q(x, t)\,\delta w\,|_0^L+Q_1\delta w_1+Q_2\delta w_2\}dt \\ &+\int_{t_1}^{t_2}\{M(x, t)\,\delta\theta\,|_0^L+M_1\delta\theta_1+M_2\delta\theta_2\}dt=0 \end{aligned} \tag{5}$$

where $Q(x, t)$ and $M(x, t)$ are the shear force and bending moment defined by

$$\begin{aligned} Q(x, t)&=-EIw'''-\rho Ac(\dot{w}+cw')+Pw' \\ M(x, t)&=-EIw'' \end{aligned} \tag{6}$$

From Eq. (5), the equation of motion for the moving BE-beam model can be obtained as

$$\begin{aligned} &EIw''''-Pw''+\rho A(\ddot{w}+2c\dot{w}'+c^2w'') \\ &=f(x, t) \end{aligned} \tag{7}$$

together with the relevant boundary conditions given by

Copyright (C) 2003 NuriMedia Co., Ltd.

$$\begin{aligned}&\{ w(0, t)=w_1 \text{ or } Q(0, t)=-Q_1 \} \text{ and}\\ &\{ \theta(0, t)=\psi_1 \text{ or } M(0, t)=M_1 \} \text{ at } x=0\\ &\{ w(L, t)=w_2 \text{ or } Q(L, t)=Q_2 \} \text{ and}\\ &\{ \theta(L, t)=\psi_2 \text{ or } M(L, t)=-M_2 \} \text{ at } x=L\end{aligned} \tag{8}$$

3. Spectral Element Formulation

The spectral element formulation begins with the governing equations of motion without external forces. The free vibration response of the moving BE-beam model are then represented in the discrete Fourier transform (DFT) forms as (Doyle, 1997 ; Lee et al., 2000)

$$w(x, t)=\sum_{n=0}^{N-1} W_n(x)\, e^{i\omega_n t} \tag{9}$$

where $i=\sqrt{-1}$ is the imaginary unit and $W_n(x)$ is the spectral components (or Fourier coefficients) corresponding to the discrete frequencies $\omega_n=2\pi n/T$ $(n=0, 1, 2, \cdots, N-1)$. N denotes the number of spectral components (often called sampling number) to be taken into account in the analysis, and T is the time window related to N as (Newland, 1993)

$$N=2f_{\mathrm{NYQ}}T \tag{10}$$

where f_{NYQ} is the highest frequency in Hz called the Nyquist frequency. Note that $W_{N-n}=W_n^*$, where W_n^* is complex conjugate of W_n by the definition of DFT. The accuracy of time responses may depend on how many spectral components are taken into account in the analysis. The summation and subscripts used in Eq. (9) are so obvious that they will be omitted in the following equations for brevity.

By substituting Eq. (9) into Eq. (7), with $f(x, t)=0$, one may obtain

$$W''''-(P_0-m^2k_0^2)\,W''+2imk_0^3W'-k_0^4W=0 \tag{11}$$

where $P_0=P/EI$, k_0 is the wave number of the stationary beam without axial tension (i.e., $c=0$ and $P=0$), and m is the dimensionless moving speed of beam (i.e., Mach number). They are defined by

$$m=\frac{c}{c_p},\ k_0=\frac{\omega}{c_p},\ c_p^2=\omega\sqrt{\frac{EI}{\rho A}} \tag{12}$$

where c_p is called the phase velocity of bending wave. The general solution of Eq. (11) (i.e., a specific spectral component) is assumed in the form

$$W(x)=Ce^{ikx} \tag{13}$$

where k is the wave number. Substituting Eq. (13) into Eq. (11) gives a dispersion relation as

$$k^4+(P_0-m^2k_0^2)\,k^2-2mk_0^3k-k_0^4=0 \tag{14}$$

Let's define dimensionless variables as

$$\begin{aligned}&\bar{k}=Lk,\ \bar{k}_0=Lk_0,\ \bar{c}=m\bar{k}_0=\sqrt{\frac{\rho A}{EI}}Lc\\ &\bar{P}=L^2P_0=\frac{L^2}{EI}P\end{aligned} \tag{15}$$

By use of the dimensionless variables, Eq. (14) can be rewritten is

$$\bar{k}^4+(\bar{P}-\bar{c}^2)\,\bar{k}^2-2\bar{c}\bar{k}_0^2\bar{k}-\bar{k}_0^4=0 \tag{16}$$

From Eq. (14), four roots k_r $(r=1, 2, 3, 4)$ can be obtained. Then the general solution of Eq. (11) can be expressed as

$$W(x)=\sum_{r=1}^{4} C_r e^{ik_r x} \tag{17}$$

Now, consider a finite beam element of length l as shown in Fig. 1. The spectral nodal degrees-of-freedom (simply, spectral nodal DOFs), spectral nodal forces and spectral nodal bending moments are listed in Fig. 1. The spectral nodal DOFs are defined by

$$\begin{aligned}&W_1=W(0),\ \Theta_1=W'(0)\\ &W_2=W(l),\ \Theta_2=W'(l)\end{aligned} \tag{18}$$

Substituting Eq. (17) into Eq. (18) gives a relation between the spectral nodal DOFs vector $\{\boldsymbol{d}\}$ and the constants vector $\{\boldsymbol{C}\}$ as

$$\{\boldsymbol{d}\}=[\boldsymbol{Y}(\omega)]\{\boldsymbol{C}\} \tag{19}$$

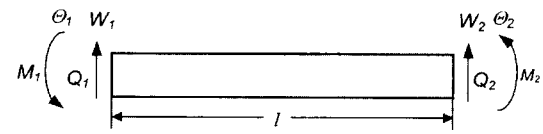

Fig. 1 Sign convention for the spectral BE-beam element model

Copyright (C) 2003 NuriMedia Co., Ltd.

where

$$\{\boldsymbol{d}\}=\{W_1\ \Theta_1\ W_2\ \Theta_2\}^T$$
$$\{\boldsymbol{C}\}=\{C_1\ C_2\ C_3\ C_4\}^T$$
$$[\boldsymbol{Y}(\omega)]=\begin{bmatrix}1 & 1 & 1 & 1\\ \varepsilon_1 & \varepsilon_2 & \varepsilon_3 & \varepsilon_4\\ e_1 & e_2 & e_3 & e_4\\ e_1\varepsilon_1 & e_2\varepsilon_2 & e_3\varepsilon_3 & e_4\varepsilon_4\end{bmatrix} \tag{20}$$

with

$$\varepsilon_r=ik_r,\ e_r=e^{ik_rl}\ (r=1,\ 2,\ 3,\ 4) \tag{21}$$

Assume the shear force $Q(x,\ t)$ and bending moment of $M(x,\ t)$ can be represented in the DFT forms as

$$Q(x,\ t)=\sum_{n=0}^{N-1}Q_n(x)\,e^{i\omega_n t}$$
$$M(x,\ t)=\sum_{n=0}^{N-1}M_n(x)\,e^{i\omega_n t} \tag{22}$$

In the following, the summation and subscripts used in Eq. (22) will be omitted for brevity. Applying Eq. (9) into Eq. (6) and using Eq. (22) may yield the spectral components of $Q(x,\ t)$ and $M(x,\ t)$ as follows

$$Q(x)=-EI[W'''-(P_0-m^2k_0^2)\,W'+imk_0^3W]$$
$$M(x)=-EIW'' \tag{23}$$

The spectral nodal shear forces and spectral nodal bending moments specified on the finite beam element (see Fig. 1) are defined by

$$Q_1=-Q(0),\ M_1=M(0)$$
$$Q_2=Q(l),\ M_2=-M(l) \tag{24}$$

Substituting Eq. (19) into Eq. (23) and applying Eq. (24) gives a relation between the spectral nodal forces vector $\{\boldsymbol{f}\}$ and the constants vector $\{\boldsymbol{C}\}$ as

$$\{\boldsymbol{f}\}=[\boldsymbol{X}(\omega)]\{\boldsymbol{C}\} \tag{25}$$

where

$$\{\boldsymbol{f}\}=\{Q_1\ M_1\ Q_2\ M_2\}^T$$
$$[X(\omega)]=EI\begin{bmatrix}-g_1 & -g_2 & -g_3 & -g_4\\ k_1^2 & k_2^2 & k_3^2 & k_4^2\\ e_1g_1 & e_2g_2 & e_3g_3 & e_4g_4\\ -e_1k_1^2 & -e_2k_2^2 & -e_3k_3^2 & -e_4k_4^2\end{bmatrix} \tag{26}$$

with

$$g_r=i[k_r^3+(P_0-m^2k_0^2)\,k_r-mk_0^3]\quad(r=1,\ 2,\ 3,\ 4) \tag{27}$$

The constants vector $\{\boldsymbol{C}\}$ can be readily eliminated from Eqs. (19) and (25) to result in the spectral nodal forces vector-spectral nodal DOFs vector relation in the form

$$\{\boldsymbol{f}\}=[\boldsymbol{s}(\omega)]\{\boldsymbol{d}\} \tag{28}$$

where $[\boldsymbol{s}(\omega)]$ is the spectral element matrix, which is the frequency-dependent Hermitian matrix defined by

$$[\boldsymbol{s}(\omega)]=[\boldsymbol{X}(\omega)][\boldsymbol{Y}(\omega)]^{-1} \tag{29}$$

The spectral element equation, Eq. (28) can be rewritten in terms of dimensionless variables as

$$\{\bar{\boldsymbol{f}}\}=[\bar{\boldsymbol{s}}(\bar{\omega})]\{\bar{\boldsymbol{d}}\} \tag{30}$$

where $\bar{\omega}$ is the dimensionless circular frequency defined by

$$\bar{\omega}=\omega L^2\sqrt{\frac{\rho A}{EI}} \tag{31}$$

and $\{\bar{\boldsymbol{f}}\}$ and $\{\bar{\boldsymbol{d}}\}$ are the dimensionless spectral nodal forces vector and spectral nodal DOFs vector, respectively, defined by

$$\{\bar{\boldsymbol{f}}\}=\{\bar{Q}_1,\ \bar{M}_1,\ \bar{Q}_2,\ \bar{M}_2\}^T$$
$$=\left\{\frac{L^2}{EI}Q_1,\ \frac{L}{EI}M_1,\ \frac{L^2}{EI}Q_2,\ \frac{L}{EI}M_2\right\}^T$$
$$\{\bar{\boldsymbol{d}}\}=\{\bar{W}_1,\ \bar{\Theta}_1,\ \bar{W}_2,\ \bar{\Theta}_2\}^T$$
$$=\left\{\frac{1}{L}W_1,\ \Theta_1,\ \frac{1}{L}W_2,\ \Theta_2\right\}^T \tag{32}$$

The dimensionless spectral element matrix $[\bar{\boldsymbol{s}}(\bar{\omega})]$ is defined by

$$[\bar{\boldsymbol{s}}(\bar{\omega})]=[\bar{\boldsymbol{X}}(\bar{\omega})][\bar{\boldsymbol{Y}}(\bar{\omega})]^{-1} \tag{33}$$

where

$$[\bar{X}(\bar{\omega})]=\begin{bmatrix}-\bar{g}_1 & -\bar{g}_2 & -\bar{g}_3 & -\bar{g}_4\\ \bar{k}_1^2 & \bar{k}_2^2 & \bar{k}_3^2 & \bar{k}_4^2\\ \bar{e}_1\bar{g}_1 & \bar{e}_2\bar{g}_2 & \bar{e}_3\bar{g}_3 & \bar{e}_4\bar{g}_4\\ -\bar{e}_1\bar{k}_1^2 & -\bar{e}_2\bar{k}_2^2 & -\bar{e}_3\bar{k}_3^2 & -\bar{e}_4\bar{k}_4^2\end{bmatrix}$$
$$[\bar{\boldsymbol{Y}}(\bar{\omega})]=\begin{bmatrix}1 & 1 & 1 & 1\\ \bar{\varepsilon}_1 & \bar{\varepsilon}_2 & \bar{\varepsilon}_3 & \bar{\varepsilon}_4\\ \bar{e}_1 & \bar{e}_2 & \bar{e}_3 & \bar{e}_4\\ \bar{e}_1\bar{\varepsilon}_1 & \bar{e}_2\bar{\varepsilon}_2 & \bar{e}_3\bar{\varepsilon}_3 & \bar{e}_4\bar{\varepsilon}_4\end{bmatrix} \tag{34}$$

with

Copyright (C) 2003 NuriMedia Co., Ltd.

$$\bar{g}_r = i[\bar{k}_r^3 + (\bar{P} - \bar{c}^2)\bar{k}_r - \bar{c}\bar{\omega}]$$
$$\bar{e}_r = e^{i\bar{k}_r \bar{l}/L},\ \bar{\varepsilon}_r = i\bar{k}_r \tag{35}$$

The spectral element matrices can be assembled in a completely analogous way to that used in FEM (Doyle, 1997 ; Lee at al., 2000). Applying the boundary conditions after the assembly may provide a global system equation in the form as

$$[\boldsymbol{S}(\omega)]\{\boldsymbol{d}_g\} = \{\boldsymbol{f}_g\} \tag{36}$$

where $[\boldsymbol{S}(\omega)]$ is the global spectral matrix (i.e., global dynamic stiffness matrix), $\{\boldsymbol{d}_g\}$ is the global spectral nodal DOFs vector, and $\{\boldsymbol{f}_g\}$ is the global spectral nodal forces vector.

To obtain the dynamic responses in time-domain, first compute $\{\boldsymbol{f}_g\}$ from the external forces transformed into the frequency-domain by using the forward FFT algorithm. Next solve Eq. (36) for $\{\boldsymbol{d}_g\}$ and apply the results into Eq. (19) to compute the spectral displacement components from Eq. (17). Finally, based on Eq. (9), the inverse FFT algorithm is used to obtain the dynamic responses in the time-domain. The natural frequencies (NAT are computed from the condition that the determinant of global spectral matrix $[\boldsymbol{S}(\omega)]$ becomes zero as follows :

$$\det[\boldsymbol{S}(\omega_{NAT})] = 0 \tag{37}$$

4. Static and Dynamic Instabilities

An axially moving beam may become unstable if its moving speed is over a certain critical speed. To investigate the stability of the moving beam one usually assumes the free vibration responses of the form (Bisplinghoff and Ashley, 1962)

$$w(x,\ t) = W(x)\, e^{\lambda t} \text{ or}$$
$$\bar{w}(\bar{x},\ \bar{t}) = \bar{W}(\bar{x})\, e^{\bar{\lambda}\bar{t}} \tag{38}$$

where $\bar{x}$, $\bar{\lambda}$, and $\bar{t}$ are the dimensionless spatial coordinate, the dimensionless eigenvalue, and the dimensionless time, respectively, defined by

$$\bar{x} = \frac{x}{L},\ \bar{t} = \frac{1}{L^2}\sqrt{\frac{EI}{\rho A}}t,\ \bar{\lambda} = \sqrt{\frac{\rho A}{EI}}L^2\lambda \tag{39}$$

Applying Eq. (38) into the free vibration equation of Eq. (7) yields an eigenvalue problem from which the dimensionless (complex) eigenvalues $\bar{\lambda}$ can be computed in the form

$$\bar{\lambda} \equiv \mathrm{Re}(\bar{\lambda}) + i\,\mathrm{Im}(\bar{\lambda}) \tag{40}$$

where $\mathrm{Re}(\bar{\lambda})$ and $\mathrm{Im}(\bar{\lambda})$ denote the real and imaginary parts of dimensionless engenvalue $\bar{\lambda}$, respectively. The type of instability can be determined from the signs of the real and imaginary parts of all dimensionless eigenvalues as follows :

Stable if $\mathrm{Re}(\bar{\lambda}) \le 0$
Unstable : static instability (divergence)
if $\mathrm{Re}(\bar{\lambda}) > 0$ and $\mathrm{Im}(\bar{\lambda}) = 0$ (41)
Unstable : dynamic instability (flutter)
if $\mathrm{Re}(\bar{\lambda}) > 0$ and $\mathrm{Im}(\bar{\lambda}) \neq 0$

The eigenvalue problem to investigate the stability of the present moving beam problem can be readily reduced from Eq. (30) by simply replacing $i\bar{\omega}$ with $\bar{\lambda}$, which can be hinted from Eq. (36) as

$$[\bar{\boldsymbol{S}}(\bar{\lambda})]\{\bar{\boldsymbol{d}}_g\} = \{\boldsymbol{0}\} \tag{42}$$

The type of instability, at a specific dimensionless moving speed $\bar{c}$ and dimensionless axial tension $\bar{P}$, is then determined by investigating the dimensionless eigenvalues $\bar{\lambda}$ numerically solved from the characteristic equation

$$\det[\bar{\boldsymbol{S}}(\bar{\lambda})] = 0 \tag{43}$$

The dimensionless wavenumbers $\bar{k}_r$ ($r = 1, 2, 3, 4$) required to compute $[\bar{\boldsymbol{S}}(\bar{\lambda})]$ in Eq. (42) are obtained from Eq. (16), with replacing $i\bar{\omega}$ with $\bar{\lambda}$.

The dimensionless critical speed at which the static instability (i.e., divergence speed $\bar{c}_D$) occurs can be derived in a closed form by considering the existence of non-trivial equilibrium position, i.e., the static eigenvalue problem (Wickert and Mote, 1990). The characteristic equation of the static eigenvalue problem can be reduced from Eq. (16) by putting $\bar{\omega} = 0$ (i.e., $\bar{k}_0 = 0$) as

$$\bar{k}^2[\bar{k}^2 + (\bar{P} - \bar{c}^2)] = 0 \tag{44}$$

Equation (44) gives four roots as

$$\bar{k}_1 = \bar{k}_2 = 0,\ \bar{k}_3 = -\bar{k}_4 = \bar{k}^* = \sqrt{\bar{c}^2 - \bar{P}} \tag{45}$$

Copyright (C) 2003 NuriMedia Co., Ltd.

Thus, the non-trivial equilibrium displacements of the moving beam can be expressed in the form

$$\bar{w}(\bar{x}) = C_1 + C_2\bar{x} + C_3 e^{ik^*x} + C_4 e^{-ik^*x} \quad (46)$$

The coefficients C_i $(i=1, 2, 3, 4)$ are determined by the boundary conditions. Applying the simply supported boundary conditions to Eq. (46) gives

$$\bar{k}_n^* = n\pi \ (n=1, 2, 3, \cdots) \quad (47)$$

where n denotes the vibration mode number. Substituting Eq. (46) into the low relation of Eq. (45) gives the dimensionless divergence speed $\bar{c}_{Dn}$, at which the divergence instability of the n-th vibration mode occurs, as follows:

$$\bar{c}_{Dn} = \sqrt{\bar{k}_n^{*2} + \bar{P}} \quad (48)$$

Equation (48) shows that, in theory, the static instability occurs whenever the dimensionless moving speed of a beam is equal to the phase speed of the propagating bending wave (i.e., $\bar{\omega}/\bar{k}_1^*$). However, in practice, the critical speed of a moving beam is considered as the dimensionless lowest divergence speed $\bar{c}_{D1}$ that is equal to the phase speed of the first propagating bending wave.

5. Numerical Illustrations and Discussions

For numerical illustrations, a simply supported uniform moving beam is considered. Table 1 is prepared to verify the high accuracy of the present spectral element model and also to investigate the effects of dimensionless moving speed $\bar{c}$ and dimensionless axial tension $\bar{P}$ on the natural frequencies. The present spectral element model is evaluated by comparing the natural frequencies obtained by SEM with those obtained by the analytical approach (Blevins, 1979) and the conventional FEM. The finite element model used in this study is formulated in the form

$$[\boldsymbol{M}]\{\ddot{\boldsymbol{d}}\} + [\boldsymbol{C}]\{\dot{\boldsymbol{d}}\} + [\boldsymbol{K}]\{\boldsymbol{d}\} = \{\boldsymbol{f}\} \quad (49)$$

Table 1 Comparison of the natural frequencies obtained by the present SEM, FEM, and analytical method (Blevins, 1979)

Dimensionless Moving Speed	Method	$N_E(N_{DOF})$	Dimensionless Natural Frequency			
			Im(λ_1)	Im(λ_2)	Im(λ_3)	Im(λ_5)
0	Analytical	1	10.361	39.974	89.328	247.237
	SEM	1 (2)	10.361	39.974	89.328	247.237
	FEM	10 (20)	10.361	39.974	89.372	248.211
		20 (40)	10.361	39.974	89.328	247.306
		50 (100)	10.361	39.974	89.328	247.237
$0.5\bar{c}_{D1}$	SEM	1 (2)	8.734	38.855	88.354	246.389
	FEM	10 (20)	8.734	38.862	88.411	247.400
		20 (40)	8.734	38.855	88.360	246.452
		50 (100)	8.734	38.855	88.354	246.389
$\bar{c}_{D1}$	SEM	1 (2)	0.000	35.337	85.414	243.825
	FEM	10 (20)	0.038	35.349	85.483	244.956
		20 (40)	0.019	35.337	85.420	243.894
		50 (100)	0.019	35.337	85.414	243.825
$\bar{c}_{F1}$	SEM	1 (2)	—	11.096	73.174	233.665
	FEM	10 (20)	—	11.322	73.318	235.274
		20 (40)	—	11.115	73.187	233.747
		50 (100)	—	11.096	73.174	233.665

Note: N_E=number of finite elements, N_{DOF}=number of degrees-of-freedom

Copyright (C) 2003 NuriMedia Co., Ltd.

where $\{\boldsymbol{d}\}$ is the nodal displacement DOF vector defined by Eq. (19), $\{\boldsymbol{f}\}$ is the nodal forces vector, $[\boldsymbol{M}]$ is the mass matrix, $[\boldsymbol{C}]$ is the skew-symmetric gyroscopic matrix, and $[\boldsymbol{K}]$ is the stiffness matrix : the finite element matrices are given in Appendix. To formulate the finite element model given by Eq. (49), the displacement fields within a finite element of length l are assumed in the form (Petyt, 1990)

$$w(x, t)=[\boldsymbol{N}(x)]\{\boldsymbol{d}(t)\} \tag{50}$$

where $[\boldsymbol{N}]$ is the shape function matrix given in Appendix.

Because the example beam is uniform, only one spectral finite element is used to obtain the SEM results in Table 1, while the total number of conventional finite elements is gradually increased to improve the FEM results. Table 1 shows that the SEM results for $\bar{c}=0$ and $\bar{P}=0$ are identical to the exact analytical results given by Blevins (1979), while the FEM results converge to the SEM results (obtained by using one spectral finite element) as the total number of conventional finite elements used in FEM is increased. This implies that, in contrast to the conventional FEM model, the present spectral element model provides highly accurate results by using only a small number of finite elements. This is true especially at high frequency modes.

From Table 1, one may observe that, for a fixed dimensionless moving speed, the dimensionless natural frequencies are in general increased as the dimensionless axial tension is increased. On the other hand, for a fixed dimensionless axial tension, all dimensionless natural frequencies are decreased as the dimensionless moving speed of beam is increased. One may also observe from Table 1 that the fundamental dimensionless natural frequency vanishes first when the dimensionless moving speed of beam $\bar{c}$ is increased to a certain critical value (i.e., divergence speed $\bar{c}_{D1}$) at which the static instability (i.e., divergence) occurs.

Figure 2 shows the changes in the dimensionless eigenvalues $\bar{\lambda}=\mathrm{Re}(\bar{\lambda})+i\mathrm{Im}(\bar{\lambda})$ with varying the dimensionless moving speed of beam $\bar{c}$, for dimensionless axial tension $\bar{P}=1$. When the dimensionless moving speed $\bar{c}$ is lower than about $\bar{c}_{D1}=3.30$ (the first divergence speed), the moving beam is stable because all dimensionless eigenvalues are pure imaginary. However, if the dimensionless moving speed is between $\bar{c}_{D1}$ and $\bar{c}_S=6.36$, there exist pure positive real eigenvalues (i.e., $\mathrm{Re}(\bar{\lambda})>0$, $i\mathrm{Im}(\bar{\lambda})=0$), which implies the occurrence of the static instability (i.e., divergence). Figure 2 shows that there exist the second stable region between $\bar{c}_S$ and $\bar{c}_{F1}=6.44$, in which all eigenvalues are pure imaginary. If the dimensionless moving speed of beam becomes larger than $\bar{c}_{F1}$, then there exist complex eigenvalues with positive real parts $\mathrm{Re}(\bar{\lambda})$, which implies the occurrence of dynamic instability (i.e., flutter). Thus $\bar{c}_{F1}=6.44$ is the lowest flutter speed of the example beam. In Fig. 2, $\bar{c}_{D2}=9.48$ is the second divergence speed and $\bar{c}_{F2}=10.30$ is the second flutter speed.

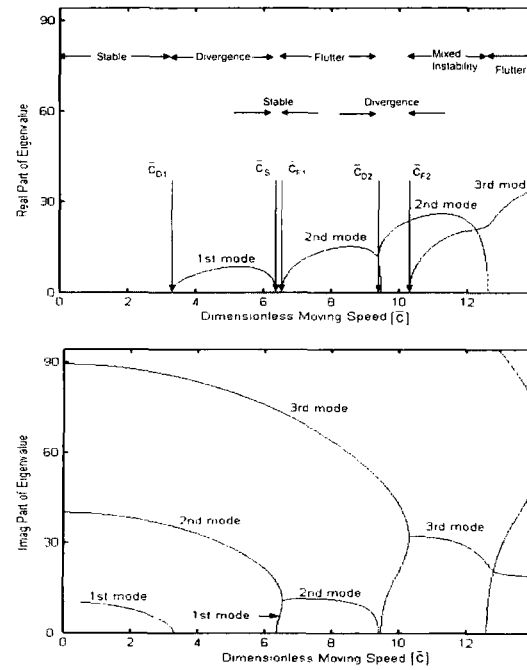

Fig. 2 The dimensionless eigenvalues $\bar{\lambda}=\mathrm{Re}(\bar{\lambda})+i\mathrm{Im}(\bar{\lambda})$ vs. the moving speed of beam $\bar{c}$, where $\bar{c}_{D1}$ is the lowest divergence speed, $\bar{c}_S$ is the moving speed at which the second stable region appears, $\bar{c}_{F1}$ is the lowest flutter speed, $\bar{c}_{D2}$ is the second divergence speed, and $\bar{c}_{F2}$ is the second flutter speed

Copyright (C) 2003 NuriMedia Co., Ltd.

Figure 3 shows the dimensionless time responses of the moving beam at various dimensionless moving speeds, when $\bar{P}=1$. The time responses are reconstructed from the spectral components of response by using the inverse FFT, represented by Eq. (9). The sampling number N used for the responses in Fig. 3 is 1024, which is chosen so as to obtain satisfactory converged results. As shown in Fig. 3(a), the moving beam is stable when it moves at $\bar{c}=1$, which is lower than the first divergence speed $\bar{c}_{D1}=3.30$. However, Fig. 3(b) shows that the moving beam indeed becomes unstable by divergence when it moves at slightly higher speed than the divergence speed $\bar{c}_{D1}$. As can be expected from Fig. 2, the moving beam becomes stable again when it moves at $\bar{c}=6.40$, which is located within the second stable zone of Fig. 2. Fig. 3(d) shows that the moving beam becomes unstable by flutter when it moves at $\bar{c}_{F1}=6.44$, which is the lowest flutter speed.

Figure 4 shows the changes in three critical dimensionless moving speeds of beam, $\bar{c}_{D1}$ (the lowest dimensionless divergence speed), $\bar{c}_S$, and $\bar{c}_{F1}$ (the lowest dimensionless flutter speed) with varying the dimensionless axial tension $\bar{P}$. The region below the curve $\bar{c}_{D1}$ and the narrow region between two curves $\bar{c}_S$ and $\bar{c}_{F1}$ are the first stable region and the second stable region, respectively. The region between two curves $\bar{c}_{D1}$ and $\bar{c}_S$ indicates the first divergence instability region, while the region just above the curve $\bar{c}_{F1}$ indicates the flutter instability region. It is apparent from Fig. 4 that the three critical dimensionless moving speeds are monotonically increased as the dimensionless axial tension is

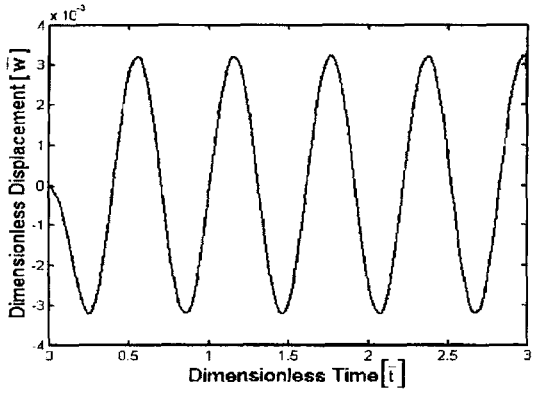

(a) When $\bar{c}=1.00$: stable

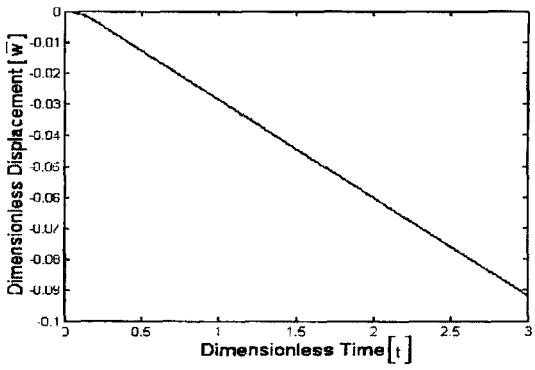

(b) When $\bar{c}=1.001$ $\bar{c}_{D1}$: divergence

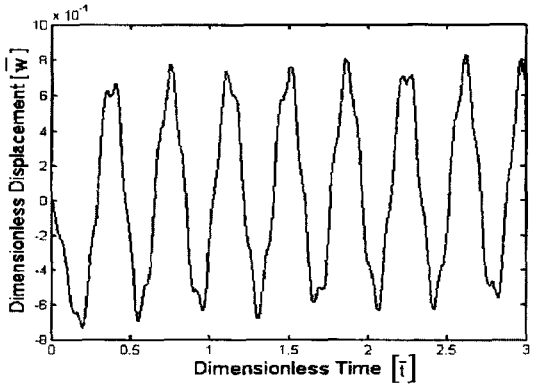

(c) When $\bar{c}=6.40$: stable

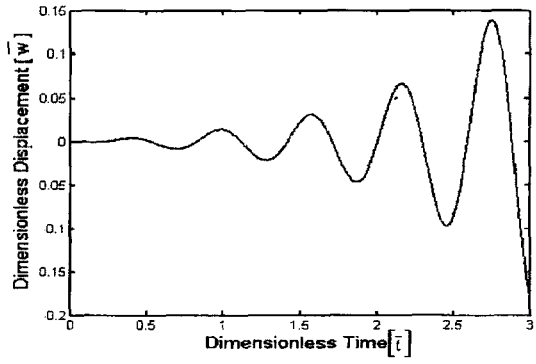

(d) When $\bar{c}_{F1}=6.44$: flutter

Fig. 3 Dimensionless time responses at various moving speeds of beam when the dimensionless axial tension is $\bar{P}=1$

Copyright (C) 2003 NuriMedia Co., Ltd.

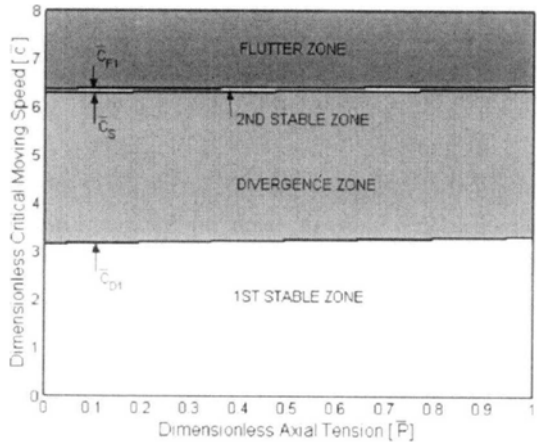

Fig. 4 The dimensionless critical moving speeds *vs.* the dimensionless axial tension, where $\bar{c}_{D1}$ is the first divergence speed, $\bar{c}_S$ is the moving speed at which the second stable region appears, and $\bar{c}_{F1}$ is the first flutter speed

increased.

Figure 5 shows the changes in the dispersion curves of the moving BE-beam model with varying its dimensionless moving speed. The lowest two dimensionless natural frequencies are indicated in Fig. 5 by the circle (O) and the triangle (Δ), in order to show they all move to leftward as the moving speed of beam is increased. As shown in Fig. 5(e), the fundamental dimensionless natural frequency $\bar{\omega}_1$ vanishes first when the dimensionless moving speed reaches at $\bar{c}_{D1}=3.30$ and then it disappears forever as the dimensionless moving speed is increased over $\bar{c}_{D1}$. When the beam is in the stationary state (i.e., $\bar{c}=0$), the dimensionless wavenumber $\bar{k}_2$ is pure imaginary. Thus, there exists evanescent wave within the beam as shown in Fig. 5(a). However, when the beam is moving, dimensionless wavenumber $\bar{k}_2$

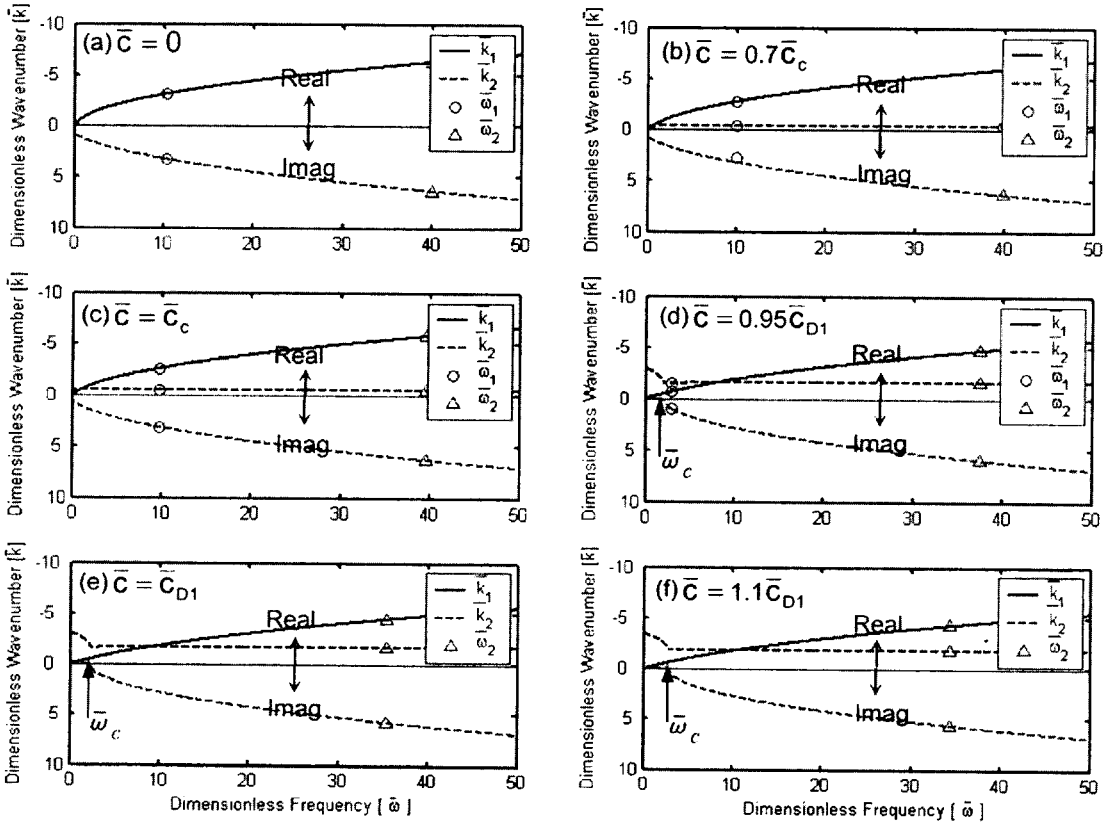

Fig. 5 Moving speed dependence of the dispersion relation of a moving BE-beam model when the dimensionless axial tension is $\bar{P}=1$. The circle (O) and the triangle (Δ), indicate the first and second natural frequencies, respectively, and $\bar{\omega}_c$ is the cut-off frequency that appears when $\bar{c} \geq \bar{c}_c$

Copyright (C) 2003 NuriMedia Co., Ltd.

becomes complex as shown in Fig. 5(b). As the moving speed of beam is increased up to $\bar{c}_c=1$, all dimensionless wavenumers at the dimensionless zero frequency merge to zero(see Fig. 5(c)). If the moving speed of beam is kept increasing over $\bar{c}_c$, the dimensionless wavenumber $\bar{k}_2$ becomes pure real at $0\leq\bar{\omega}\leq\bar{\omega}_c$, while it is complex at $\bar{\omega}_c>\bar{\omega}$. This implies that, when the dimensionless moving speed is lager than $\bar{c}_c$, the original evanescent wave becomes a traveling wave within a narrow low frequency band given by $0\leq\bar{\omega}\leq\bar{\omega}_c$. Thus the dimensionless frequency $\bar{\omega}_c$ is the dimensionless cut-off frequency. The dimensionless cut-off frequency $\bar{\omega}_c$ and the dimensionless critical moving speed $\bar{c}_c$ above that the dimensionless cut-off frequency may exist can be derived from Eq. (16) as follows:

$$\bar{\omega}_c=-\frac{1}{32}\left(f_1+\sqrt{f_1^2-64f_2}\right),\ \bar{c}_c=\sqrt{\bar{P}} \qquad (51)$$

where

$$f_1=8(\bar{c}^2-\bar{P})-36(\bar{c}^2-\bar{P})\bar{c}^2+27\bar{c}^4$$
$$f_2=-\bar{P}(\bar{c}^2-\bar{P})^3 \qquad (52)$$

Figure 6 compares the natural modes of the dimensionless moving beam for various dimensionless moving speeds. It shows that the symmetric or anti-symmetric natural modes of the stationary beam are all distorted due to the effects of moving speed and their original symmetry or anti-symmetry cannot be reserved for the moving beam. In Table 1, it is shown that the fundamental natural frequency of bending mode vanishes when the moving speed of beam reaches at the divergence speed $\bar{c}_{D1}$. Accordingly, one may observe from Fig. 6(a) that the first bending mode indeed disappears when the beam is traveling at the dimensionless moving speed of $\bar{c}_{D1}$.

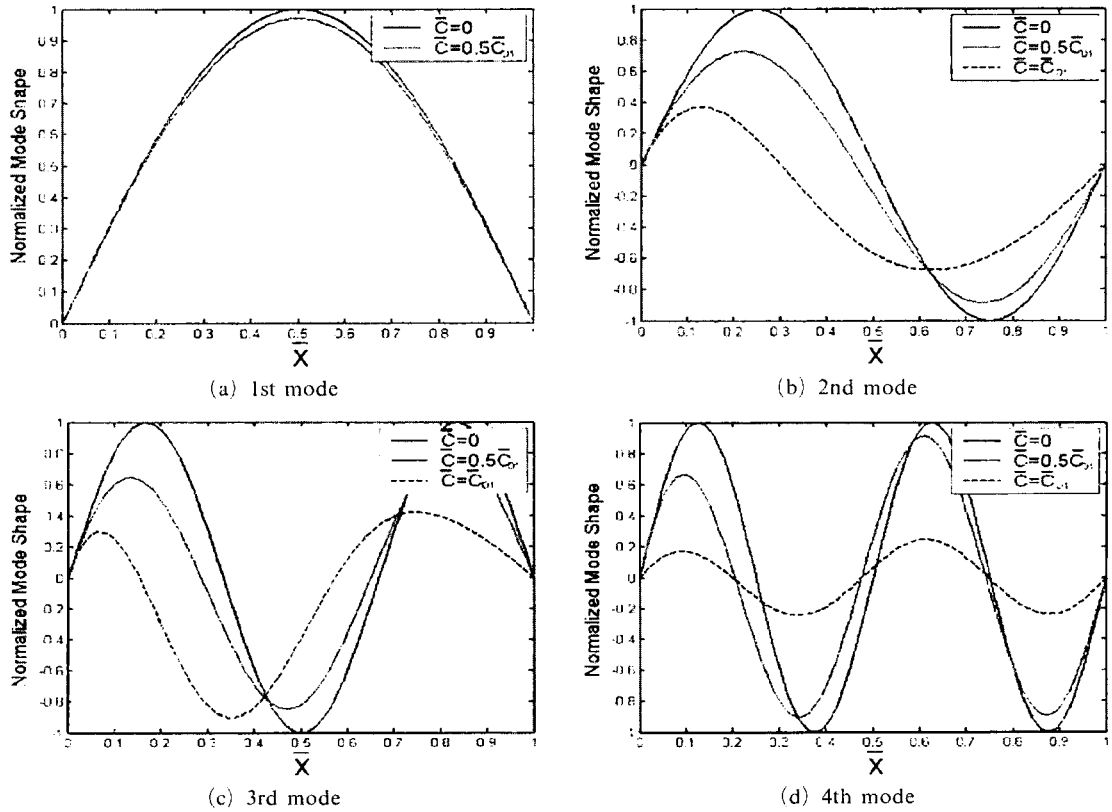

(a) 1st mode (b) 2nd mode

(c) 3rd mode (d) 4th mode

Fig. 6 Moving speed dependence of the natural modes of a moving BE-beam model when the dimensionless axial tension is $\bar{P}=1$

Copyright (C) 2003 NuriMedia Co., Ltd.

6. Conclusions

In this paper, the dynamic equations of motion for the moving BE-beam model subjected to an axial tension are derived and then the spectral element model is formulated by using the exact dynamic shape functions. The high accuracy of the spectral element is then verified by comparing its solutions with the exact analytical solutions and conventional FEM solutions. The critical moving speed at which the divergence instability occurs is analytically derived in a closed form. Through some numerical studies, the followings are investigated.

(1) When the moving speed reaches the lowest divergence speed, the first natural frequency vanishes and the first bending mode disappears, resulting in the divergence.

(2) The divergence and flutter speeds tend to increase as the axial tension is increased, and there may exist a very narrow stable region between the first divergence zone and the first flutter zone.

(3) When the beam moves at a speed larger than $\sqrt{P/\rho A}$, there appears a cut-off frequency below which the original evanescent wave becomes a propagating wave.

References

Al-Jawi, A. A. N., Pierre, C. and Ulsoy, A. G., 1995, "Vibration Localization in Dual-Span Axially Moving Beams, Part I: Formulation and Results," *Journal of Sound and Vibration*, Vol. 179, No. 2, pp. 243~266.

Bisplinghoff, R. L. and Ashley, H., 1962, *Principles of Aeroelasticity*, Dover Publication, New York.

Blevins, R. D., 1979, *Formulas for Natural Frequency and Mode Shape*, Van Nostrand Reinhold Company, New York.

Chonan, S., 1986, "Steady State Response of An Axially Moving Strip Subjected to A Stationary Lateral Load," *Journal of Sound and Vibration*, Vol. 107, No. 1, pp. 155~165.

Doyle, J. F., 1997, *Wave Propagation in Structures : Spectral Analysis Using Fast Discrete Fourier Transforms*, Springer-Verlag, New York.

Hwang, S. J. and Perkins, N. C., 1992, "Supercritical Stability of An Axially Moving Beam," *Journal of Sound and Vibration*, Vol. 154, No. 3, pp. 381~409.

Lee, H. P., 1993, "Dynamics of A Beam Moving Over Multiple Supports," *International Journal of Solids and Structures*, Vol. 30, No. 2, pp. 199~209.

Lee, U. and Lee, J., 1998, "Vibration Analysis of the Plates Subject to Distributed Dynamic Loads by Using Spectral Element Method," *KSME International Journal*, Vol. 12, No. 4, pp. 565~571.

Lee, U., Kim, J. and Leung, A. Y. T., 2000, "The Spectral Element Method in Structural Dynamics," *The Shock and Vibration Digest*, Vol. 32, No. 6, pp. 451~465.

Lee, U., Kim, J. and Leung, A. Y. T., 2001, "Vibration Analysis of the Active Multi-Layer Beams by Using Spectrally Formulated Exact Natural Modes," *KSME International Journal*, Vol. 15, No. 2, pp. 199~209.

Le-Ngoc, L. and McCallion, H., 1999, "Dynamic Stiffness of An Axially Moving String," *Journal of Sound and Vibration*, Vol. 220, No. 4, pp. 749~756.

Newland, D. E., 1993, *Random Vibrations, Spectral and Wavelet Analysis*, 3rd ed., Longman, New York.

Öz, H. R., 2001, "On the Vibrations of An Axially Traveling Beam on Fixed Supports with Variable Velocity," *Journal of Sound and Vibration*, Vol. 239, No. 3, pp. 556~564.

Pellicano, F. and Vestroni, F., 2001, "Nonlinear Dynamics and Bifurcations of An Axially Moving Beam," *Journal of Vibration and Acoustics*, Vol. 22, pp. 21~30.

Petyt, M., 1990, *Introduction to Finite Element Vibration Analysis*, Cambridge University Press, New York.

Riedel, C. H. and Tan, C. A., 1998, "Dynamic Characteristics and Mode Localization of Elastically Constrained Axially Moving Strings and Beams," *Journal of Sound and Vibration*, Vol. 215, No. 3, pp. 455~473.

Copyright (C) 2003 NuriMedia Co., Ltd.

Stylianou, M. and Tabarrok, B., 1994, "Finite Element Analysis of An Axially Moving Beam, Part I : Time Integration," *Journal of Sound and Vibration*, Vol. 178, No. 4, pp. 433~453.

Wickert, J. A. and Mote, C. D., 1988, "Current Research on the Vibration and Stability of Axially Moving Materials," *Shock and Vibration Digest*, Vol. 20, pp. 3~13.

Wickert, J. A. and Mote, C. D., 1990, "Classical Vibration Analysis of Axially Moving Continua," *Journal of Applied Mechanics*, Vol. 57, pp. 738~744.

Appendix

The shape function matrix in Eq. (50) and the finite element matrices in Eq. (49) are given by

$$[N(x)]=[1-3\xi^2+2\xi^3,\ \xi(\xi-1)^2 l,\ 3\xi^2-2\xi^3,\ \xi(\xi^2-\xi)^2 l]$$

$$[M]=\frac{\rho A l}{420}\begin{bmatrix} 156 & 22l & 54 & -13l \\ 22l & 4l^2 & 13l & -3l^2 \\ 54 & 13l & 156 & -22l \\ -13l & -3l^2 & -22l & 4l^2 \end{bmatrix}$$

$$[K]=\frac{EI}{30}\begin{bmatrix} 360+36r-36s & & \text{symmetric} & \\ 180l+3rl-3sl & 120l^2+4rl^2-4sl^2 & & \\ -360-36r+36s & -180l-3rl+3sl & 360+36r-36s & \\ 180l+3rl-3sl & 60l^2-rl^2+sl^2 & -180l-3rl+3sl & 120l^2+4rl^2-4sl^2 \end{bmatrix}$$

$$[C]=\frac{\rho A c}{30}\begin{bmatrix} 0 & 6l & 30 & -6l \\ -6l & 0 & 6l & -l^2 \\ -30 & -6l & 0 & 6l \\ 6l & l^2 & -6l & 0 \end{bmatrix}$$

where

$$\xi=2\left(\frac{x}{l}\right)-1\ (0\le x\le l),\ r=\frac{Pl^2}{EI},\ s=\frac{\rho A c^2 l^2}{EI}$$

Copyright (C) 2003 NuriMedia Co., Ltd.